Journal of the European Ceramic Society 22 (2002) 963–971

www.elsevier.com/locate/jeurceramsoc

Microstructure and mechanical properties of superplastically deformed silicon nitride–silicon oxynitride in situ composites

Rong-Jun Xie[a,b], Mamoru Mitomo[a,*], Fang-Fang Xu[a], Guo-Dong Zhan[c], Yoshio Bando[a], Yoshio Akimune[b]

[a]*Advanced Materials Laboratory, National Institute for Materials Science, Namiki 1-1, Tsukuba, Ibaraki 305-0044, Japan*
[b]*Smart Structure Research Center, National Institute of Advanced Industrial Science and Technology, Umezono 1-1-1, Tsukuba Central 2, Tsukuba, Ibaraki 305-8564, Japan*
[c]*Department of Chemical Engineering and Materials Science, University of California, Davis, One Shields Avenue, Davis, CA 95616, USA*

Received 7 March 2001; received in revised form 29 June 2001; accepted 9 July 2001

Abstract

Silicon nitride–silicon oxynitride in situ composites were fabricated by plane-strain-compressing dense silicon nitrides, starting from 93 wt.% ultrafine β-Si_3N_4 and 7 wt.% cordierite, at 1600 °C under a constant load of 40 MPa and subsequent annealing at 1750 °C for 30 min. The resulting composites featured a microstructure of elongated Si_2N_2O grains (~0.64 μm in diameter and ~5.5 in aspect ratio) dispersed in a fine-grained β-Si_3N_4 matrix (~ 0.30μm in diameter and ~3.5 in aspect ratio), with the amount of Si_2N_2O, which had relatively strong textures, being strain-dependent. The mechanical properties were found to be improved due to the development of elongated Si_2N_2O grains, the texture formation, and the coarsening of β-Si_3N_4. Fracture toughness, however, was still low (~5.2 MPa $m^{1/2}$) for these composites in comparison to self-reinforced silicon nitrides, resulted from the strong Si_2N_2O-matrix interfacial bond and nearly equiaxed β-Si_3N_4 with a small grain size. Anticipated property anisotropies were clearly observed as a result of the textured microstructure.

Keywords: Anisotropy; Composites; Mechanical properties; Microstructure-final; Si_2N_2O; Si_3N_4

1. Introduction

Silicon nitride (Si_3N_4) ceramic is one of the most promising materials for high-temperature structural applications because of excellent thermomechanical properties, such as high elevated-temperature strength, low coefficient of thermal expansion, and high resistance to thermal shock and chemical attack. The intrinsic brittleness and hardness of silicon nitride ceramic, however, make it difficult and costly to machine them into complex-shaped components. Now things are changing since Chen et al.[1] and Wakai et al.[2] independently discovered superplastic-like behavior in silicon nitride ceramics in 1990. Superplasticity offers the potential to form these ceramics into complex near-net-shaped components, which can reduce the extremely expensive and challenging issues associated with the machining of ceramics. A number of researchers have demonstrated superplasticity in several silicon nitride ceramics by applying the transient liquid phase,[3–7] using ultrafine β-phase powder,[8–13] or by adding secondary phases into Si_3N_4 to refine the microstructure.[2,14] Chen et al.[1,3,5,15] and Mitomo et al.[8] have practiced the fabrication of ceramic bodies by superplastic forming techniques. Moreover, it has been found that rather than being detrimental to the mechanical properties of silicon nitrides, superplastic deformation actually enhances them.[5,13,16]

By using ultrafine β-phase powder and applying the transient liquid phase approach, we have developed superplastic silicon nitride–silicon oxynitride in situ composites that can be uniaxially compressed at 1550 °C to large strains under higher strain rates (10^{-4}–10^{-3} 1/s) and exhibit Newtonian-flow behavior.[12,13] The resultant composites are two-phase ceramics containing Si_2N_2O, which has superior high-temperature stability and oxidation resistance,[17–20] and β-Si_3N_4. It is well known that Si_2N_2O shows certain typical growth features, tending to grow into elongated grains,[21–24] which results in the composites having a microstructure of fine-grained

* Corresponding author. Fax: +81-298-52-7449.
E-mail address: mitomo.mamoru@nims.go.jp (M. Mitomo).

0955-2219/02/$ - see front matter
PII: S0955-2219(01)00401-0

β-Si_3N_4 dispersed with rod-like Si_2N_2O grains. This structure is analogous to self-reinforced silicon nitrides,[25–27] and is functionally compatible in terms of both the thermal and mechanical properties. Moreover, the in situ development of elongated Si_2N_2O grains in the fine-grained matrix avoids the challenging problems associated with manufacturing whisker-reinforced ceramic composites, including the high cost of whiskers, the potential hazards in their handling and processing difficulties such as deagglomerating, mixing and settling. More interestingly, the applied stress during superplastic deformation biases the alignment of the elongated Si_2N_2O grains formed in situ,[28] leading to textured microstructures which are usually produced by slurry-based techniques (e.g. tape-casting, slip-casting, extrusion).[29–32] However, although reduced sinterability and sintering anisotropy are often encountered with these slurry-based techniques,[32] the present composite material has good sinterability.

In contrast to the extensive investigations of the microstructural aspects and the property optimization of composites system based on α- and β-sialon, and the efforts of sintering bulk Si_2N_2O or O′-sialons,[20,33–35] systematic investigations of composite systems based on β- and Si_2N_2O phases, and especially those concerned with their mechanical properties, are scarce in the literature.[36–38] Xu et al.[23] demonstrated that the addition of O′-sialon to a fine-grained β-sialon matrix deteriorated the strength and toughness of the matrix although it improved oxidation resistance. Our preliminary results[13,38] indicated that elongated Si_2N_2O grains could toughen and strengthen the fine-grained β-Si_3N_4 matrix, which is in direct contrast to Xu's results. Therefore, to examine the microstructure–property relationship in the Si_3N_4–Si_2N_2O composite systems and to identify an optimum microstructure in terms of a desirable property combination of mechanical properties, in the present study we develop the Si_3N_4–Si_2N_2O in situ composites mainly by superplastic deformation, and investigate their microstructural evolutions and mechanical properties.

2. Experimental procedures

The starting materials were 93 wt.% ultrafine β-Si_3N_4 (Denki Kagaku Kogyo K.K., Japan, SN-BF97M) with an average particle size of 0.20 μm, and 7 wt.% cordierite ($2MgO\ 2Al_2O_3\ 5SiO_2$ Marusu-yuyaku Co., Nagano, Japan, SS600). The β-Si_3N_4 starting powder contained 1.38% oxygen due to the presence of silica on its surface. The powder mixture was ball-milled in *n*-hexane for 2 h using silicon nitride balls. Hot-pressed Si_3N_4 was prepared using loose powder in a graphite die with a pressure of 20 MPa at 1750 °C for 5 min under 1 atm of nitrogen, and the density of the sintered Si_3N_4 was greater than 97% theoretical density determined by the Archimedes' method. This demonstrates that the densification process was dominated by particle rearrangement using the ultrafine β-Si_3N_4 powder with a narrow particle size distribution and no α→β phase transformation, thus enabling the material to reach equilibrium after a relatively low temperature.

Superplastically deformed Si_3N_4 was produced by pressing a sintered billet with a length of 21 mm in a channel graphite die of $21\times25\ mm^2$ using a constant load of 40 MPa at 1600 °C to obtain true strains ranging from 0.30 to 0.95 for 25–120 min. The deformed samples were subsequently annealed at 1750 °C for 30 min.

Fracture toughness was measured by the indentation method with loads of 98 N and calculated according to the procedures given by Marshall.[39] Flexural strength measurements were made by four-point bending tests with $2.5\times3.0\times25$ mm specimens loaded on 10 mm inner spans and supported by 20 mm outer spans. The crosshead speed was 0.5 mm/min. The tensile surface of the test bars was polished to 1 μm finish, and the edges of the tensile surface were beveled and polished to avoid stress concentrations during testing.

Microstructures were observed using scanning electron microscopy (SEM) and transmission electron microscopy (TEM). SEM samples were prepared by cutting, machining, polishing and plasma-etching with CF_4 containing 7.8 wt.% O_2. Thin foils for TEM observations were first cut and then prepared by the standard procedures of grinding, dimpling and argon-ion-beam thinning, followed by carbon coating to avoid charging during observation. The grain sizes of both β-Si_3N_4 and Si_2N_2O were determined by the method reported elsewhere.[38] A total of 500 grains of each β-Si_3N_4 and Si_2N_2O were selected from SEM micrographs taken from the surfaces parallel to the compressive stress axis, and their lengths (L), widths (D) and aspect ratio ($\lambda = L/D$) were measured using an image analyzer (Luzex ifi, Nireco Co., Tokyo, Japan).

3. Results and discussion

3.1. General microstructure characterization

Typical microstructures before and after superplastic deformation are shown in Fig. 1. This clearly shows that significant microstructural development took place during deformation. The as-sintered sample features a homogeneous microstructure, with mostly equiaxed β-Si_3N_4 grains having an average grain diameter of 0.17 ± 0.03 μm surrounded by a silica-rich grain-boundary phase. The superplastically deformed materials, however, exhibit a distinct "bimodal" microstructure, with relatively large elongated Si_2N_2O grains grown in situ dispersed in a fine-grained β-Si_3N_4 matrix. Morphologically, the Si_3N_4–Si_2N_2O in situ composites are analogous to self-reinforced

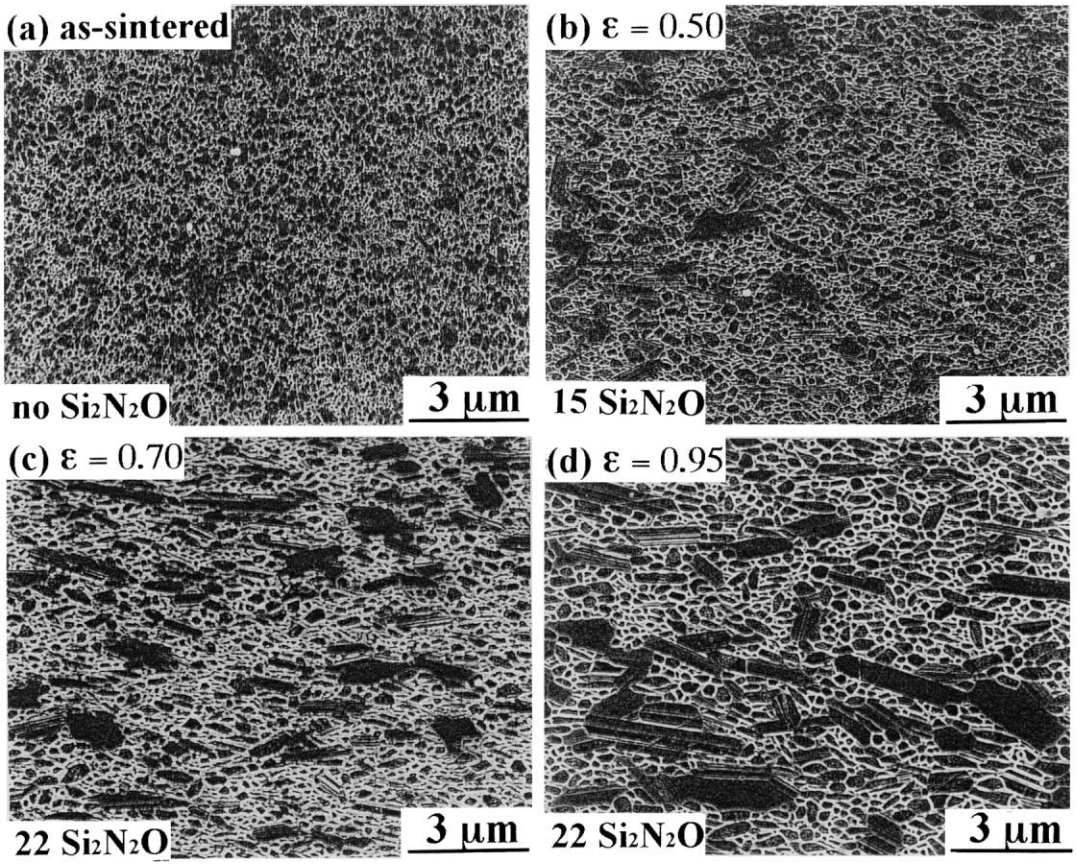

Fig. 1. SEM micrographs of (a) as-sintered, and superplastically deformed and subsequently annealed samples with (b) $\varepsilon = 0.50$, (c) $\varepsilon = 0.70$ and (d) $\varepsilon = 0.95$. It shows the in-situ development of silicon oxynitride, texture formation and the coarsening of β-silicon nitride.

silicon nitrides, with the elongated Si_2N_2O acting as the reinforcement. Increases in the volume fraction of Si_2N_2O with strain are clearly evident in the micrographs, except when a true strain of 0.70 was achieved. In those samples, the Si_2N_2O content remained at a level of 22 vol.%, which indicates that phase equilibrium was achieved. At the same time, the grain morphology and the orientation of Si_2N_2O and Si_3N_4 also changed as deformation proceeded, as will be shown below.

It is worth noting that some preferred orientations of the elongated Si_2N_2O and β-Si_3N_4 developed in the microstructure after compression and remain unchanged after annealing. This can be clearly seen in Fig. 1(c) and (d) for Si_2N_2O, but it is hard to detect texture in the β-Si_3N_4 grains from the SEM images because of their nearly equiaxed shape. A detailed description of the texture development in Si_2N_2O and β-Si_3N_4 is available in Ref. 28 based on XRD patterns and pole figure data, only a summary is provided here. Both Si_2N_2O and β-Si_3N_4 are preferentially orientated after deformation, and the degree of texture is dependent on the compressive strain. Specifically, Si_2N_2O grains are strongly textured compared to β-Si_3N_4 grains, with a texture intensity being 8 times random in the (200) pole figure for Si_2N_2O in a sample deformed to 0.95. Both Si_2N_2O and β-Si_3N_4 grains tend to align their length directions (i.e. *c*-axis for β-Si_3N_4 and *b*-axis for Si_2N_2O) normal to the compressive stress axis. The textured microstructure is believed to exert an influence on the mechanical properties of silicon nitride–silicon oxynitride in situ composites.

Fig. 2 shows the grain size and grain morphology of β-Si_3N_4 and Si_2N_2O as a function of compressive strain. Generally, the growth of β-Si_3N_4 grains is sluggish during superplastic deformation and subsequent annealing. For example, the sample compressed to a large true strain of 0.95 has an average grain diameter of 0.30±0.05 μm,

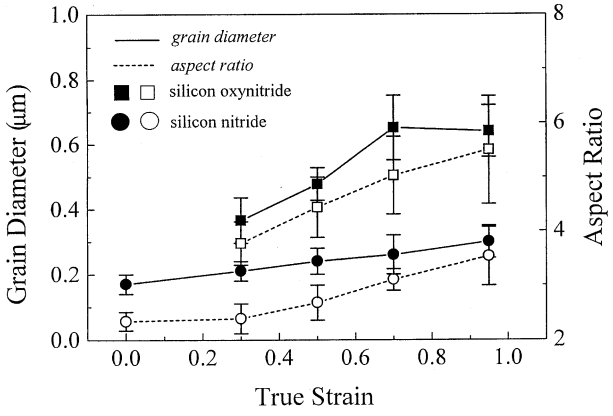

Fig. 2. Grain diameter and aspect ratio of Si_2N_2O and β-Si_3N_4 as a function of true compressive strain.

which is less than 2 times that for the as-sintered sample. Moreover, the grain shape of β-Si_3N_4 changes very little, with the aspect ratio increasing from 2.3 for the as-sintered sample to 3.5 for the sample deformed to 0.95, which represents a slight elongation of β-Si_3N_4. This quantitative image analysis indicates that the β-Si_3N_4 matrix has a low growth rate and exhibits good microstructural stability. This result is in strong contrast to that reported for superplastic sialon by Wu and Chen,[3] but is consistent with our previous studies of other fine-grained β-Si_3N_4 ceramics.[8,10–13] Wu and Chen[3] demonstrated markedly strain-induced grain growth of β-sialon under tension, leading to the development of rod-like β-sialon grains and a wire texture. They attributed the enhanced growth to grain coalescence and the lack of impingement in the presence of a large amount of transient liquid (~20 vol.%). In the present study, although a large compressive strain was achieved and a higher annealing temperature was applied, the growth rate of β-Si_3N_4 was still low. This is predominantly due to the use of ultrafine β-phase as the starting powder. The absence of α- to β-phase transformation and a narrow particle size distribution account for the low growth rate of β-Si_3N_4 and thus the small grain size.

The grain growth of Si_2N_2O, however, was pronounced and dependent on the compressive strain. The average grain diameters of Si_2N_2O are 0.37 ± 0.07, 0.48 ± 0.05 and 0.64 ± 0.08 μm for the materials deformed to 0.30, 0.55 and 0.95, respectively. Accompanying the coarsening, the Si_2N_2O grains grow anisotropically, yielding an elongated or rod-like grain morphology, as shown in Fig. 1 (b)–(d). The aspect ratio of Si_2N_2O increased from 3.8 to 5.5 for the samples deformed to 0.30 and 0.95. The development of Si_2N_2O in the β-Si_3N_4 matrix is based on the following chemical reaction: β-Si_3N_4(s) + SiO_2(l) → 2 Si_2N_2O (s), and the growth of Si_2N_2O follows an interface-reaction-controlled solution–precipitation mechanism. The grain morphology depends on its growth feature and the viscosity of the silica-rich liquid. Wang et al.[24] demonstrated that Si_2N_2O has a strong tendency to grow anisotropically with a growth speed in the [010] direction 6 times that in the [100] direction. Braue et al.[21] observed that the growth from low-viscous liquids resulted in a well-defined grain morphology exhibiting macroscopic low-index faces. In the present case, the applied stress, the presence of transient liquid and the low-viscous liquid (Mg–Al–Si–O–N) allowed the Si_2N_2O grains to grow preferentially along the [010] direction and finally develop a rod-like morphology.

3.2. Si_2N_2O crystals and the Si_2N_2O–Si_3N_4 grain boundary

Fig. 3 is a bright-field TEM image of a Si_2N_2O grain embedded in the fine-grained β-Si_3N_4 matrix. As can be seen, a large number of small round-shaped β-Si_3N_4 particles are entrapped in the Si_2N_2O grain. Electron diffraction analysis (inset B) clearly confirms that these inclusions are β-Si_3N_4. Furthermore, a high density of stacking faults is situated in the middle of Si_2N_2O, as also evidenced by the [011] diffraction pattern (inset A). Wang et al.[24] suggested that the trapping of β-Si_3N_4 particles and the development of stacking faults are associated with the higher initial grain-growth speed of Si_2N_2O. The entrapment of Si_3N_4 particles within Si_2N_2O or O′-sialon has been well documented in the literature.[21,23,24]

Fig. 4(a) is a dark-field TEM image of Si_2N_2O–Si_3N_4 grain boundaries, which highlights the amorphous phase (white contrast). Extensive TEM observations reveal that a thin amorphous layer is generally present at Si_2N_2O–Si_3N_4 grain boundaries. Fig. 4(b) shows a HRTEM lattice image of the grain boundary between Si_2N_2O and the β-Si_3N_4 matrix. The grain boundary has an intergranular amorphous film with a non-uniform thickness, suggesting the heterogeneous nucleation of Si_2N_2O on β-Si_3N_4.[24] The maximum thickness of this film is around 0.60 nm. This contrasts markedly with the grain boundary between β-Si_3N_4 grains, which either has an amorphous film with a uniform thickness in the range of 1.0–2.0 nm or is free of any amorphous films.[24,40,41]

3.3. Fracture toughness

The measured fracture toughness of the silicon nitride-silicon oxynitride in situ composites as a function of true strain is plotted in Fig. 5. Three different types of fracture toughness were investigated. Clearly, the fracture toughness increases continuously with increasing strain when it was measured along the crack propagation directions of type I and type II, with the toughness increasing from 2.93 ± 0.19 MPa $m^{1/2}$ for the

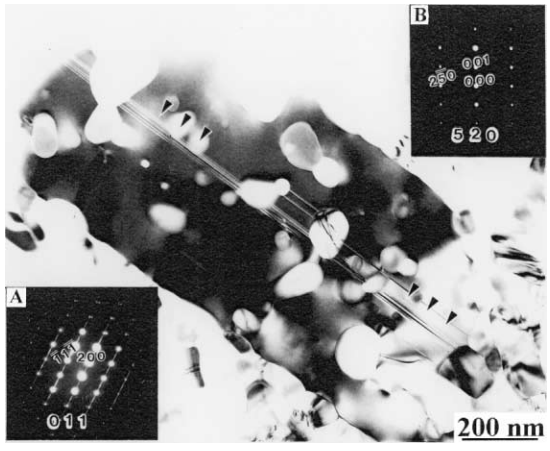

Fig. 3. TEM image (bright field) of the sampled deformed to 0.70 shows the general features of a Si_2N_2O with elongated morphology; trapping of spherical β-Si_3N_4 particles; and high density of stacking faults (indicated by triangles). Insets A and B are [011] and [520] diffraction patterns for Si_2N_2O and the entrapped β-Si_3N_4, respectively.

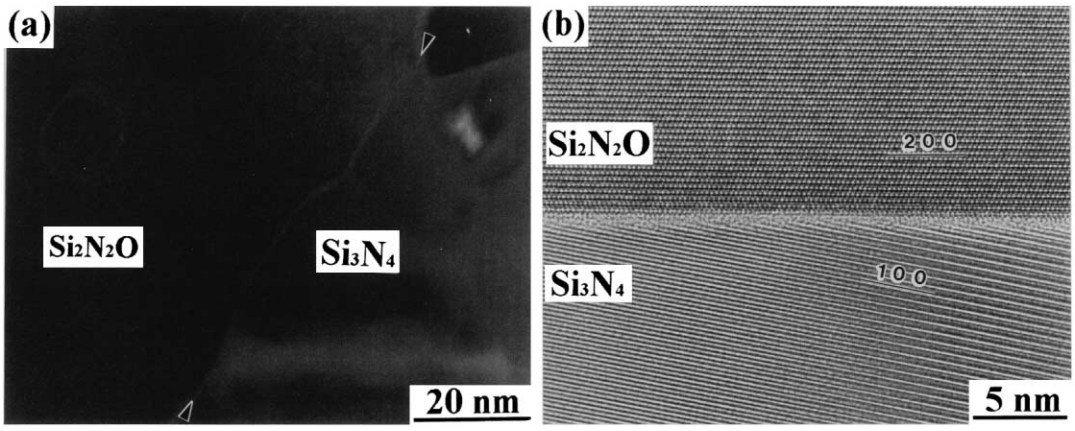

Fig. 4. (a) Low-magnification TEM image (dark field) of the sample deformed to 0.70 shows an amorphous phase in between Si_2N_2O and Si_3N_4 grains, and (b) HRTEM image shows the phase boundary between Si_2N_2O and a matrix β-Si_3N_4 grain, revealing a layer of glassy film of nonuniform thickness.

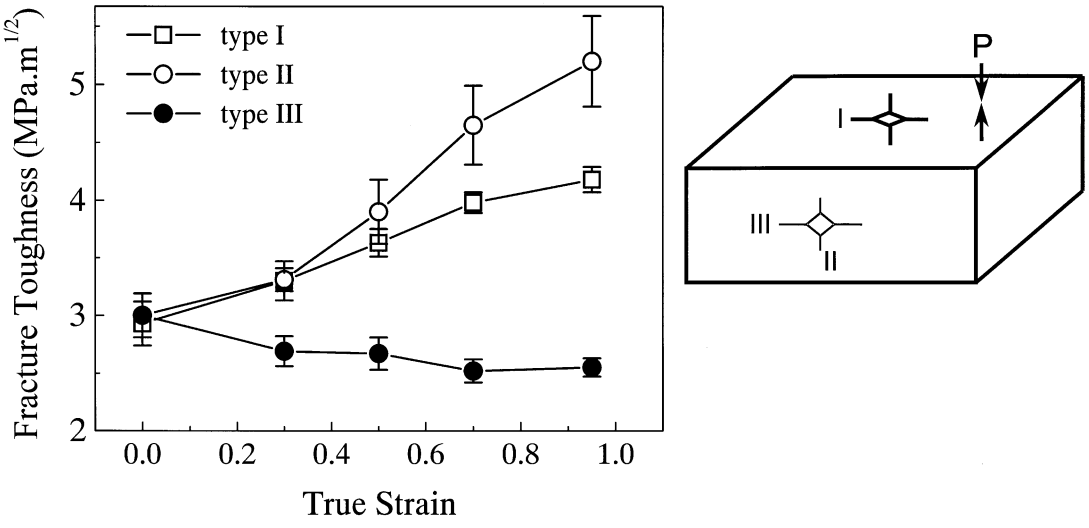

Fig. 5. Measured fracture toughness as a function of true compressive strain.

as-sintered sample to 4.18±0.10 MPa $m^{1/2}$ (type I) and 5.20±0.39 MPa $m^{1/2}$ (type II) for the sample deformed to 0.95. In contrast, the toughness drops slightly with increasing strain along the type III crack propagation direction, being 2.50±MPa $m^{1/2}$ for the sample deformed to 0.95. A fracture toughness anisotropy is observed for all the deformed samples. By comparing types I and II, as well as types I and III, fracture toughness measurements, it is apparent that the toughness anisotropy is more significant on different crack planes than on the same crack plane with different propagation directions. On the other hand, the degree of toughness anisotropy appears to be strain dependent: a larger strain results in a stronger toughness anisotropy.

Fig. 6 presents typical crack paths caused by indentation loading in the as-sintered sample and the sample deformed to 0.70. From a comparison of the interactions of the propagating cracks with the grains, the effect of the elongated Si_2N_2O grains on the crack plane is evident. The crack plane in the as-sintered sample, which contains equiaxed β-Si_3N_4 grains, remains planar throughout propagation. However, in the deformed sample containing elongated Si_2N_2O grains, it shows an extremely jagged crack path that circumvents the rod-like Si_2N_2O grains by deflection, except where Si_2N_2O was orientated normal to the crack plane. In these cases, the interface debonding energy was apparently sufficiently high that pullout could not occur, and Si_2N_2O fractured transgranularly.

Considering the microstructure evolutions and the crack profiles in the present material, the above results imply that silicon nitride–silicon oxynitride in situ composites are mainly toughened by the elongated Si_2N_2O grains, which favor a crack deflection mechanism. Of course, the coarsening of the β-Si_3N_4 matrix must have contributed to the increment in fracture toughness either by crack deflection or crack bridging as shown in Fig. 6(b). However this contribution is believed to be

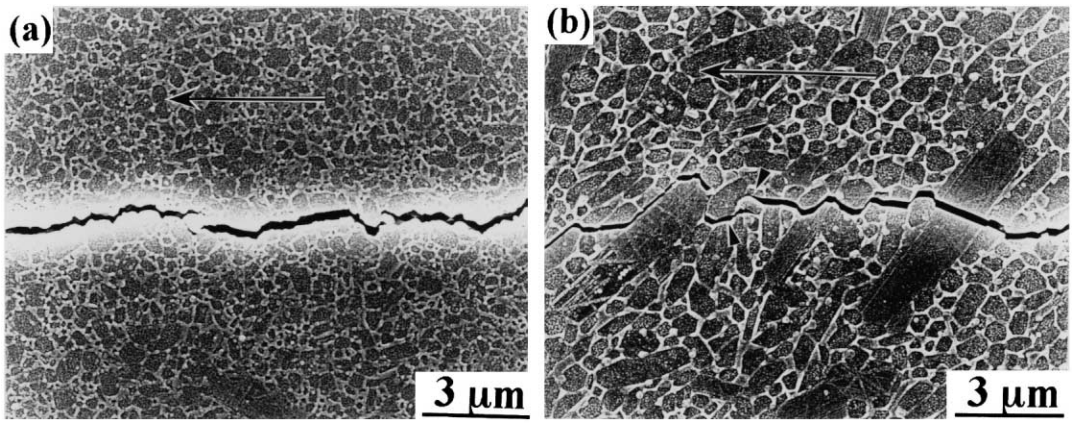

Fig. 6. Crack propagation paths in (a) as-sintered sample and (b) sample deformed to 0.70. The arrows indicate the directions of crack propagation.

small compared to Si_2N_2O because of the relatively small grain size of β-Si_3N_4. Fracture mechanics models[42,43] predict that the toughening associated with crack deflection should be particle-size invariant but highly dependent on the morphology and volume fraction of the deflecting grains. In particular, elongated grains should be more effective at toughening than equiaxed grains. In the present composites, we have observed that both the amount and the grain size of Si_2N_2O increase as the compressive strain increases, and, in particular, its aspect ratio increases up to 5.5 for largely deformed samples. This means that more and more Si_2N_2O grains are involved in the toughening process and the effect of toughening becomes much remarkable as Si_2N_2O develops into an elongated shape, which accounts for the improved fracture toughness in the largely deformed samples.

It must be acknowledged that the fracture toughness of the present silicon nitride–silicon oxynitride in situ composites is still rather low compared to self-reinforced silicon nitrides. Li and Yamanis[26] demonstrated that silicon nitrides containing large ($\geqslant$1 μm diameter) elongated grains can exhibit steady-state toughness values approaching 10 MPa $m^{1/2}$. Steep R-curves and a similar toughness value of about 10 MPa $m^{1/2}$ were also reported by Becher et al.[44] for self-reinforced silicon nitrides. We suggest the following two reasons for this difference. Firstly, the silicon nitride–silicon oxynitride in situ composites show minimal evidence of crack bridging and grain pullout of the elongated Si_2N_2O grains in the region behind the crack tips which are two dominant toughening mechanisms operating in self-reinforced silicon nitrides. Only the crack-deflection mechanism contributed to the improved fracture toughness. Furthermore, evidence of cracks propagating directly through Si_2N_2O is common. These observations indicate that a strong Si_2N_2O–Si_3N_4 interfacial bond develops in these composites. Secondly, the β-Si_3N_4 matrix exhibits fairly good microstructure stability. β-Si_3N_4 grains have a relatively small grain size and nearly equiaxed grain morphology. According to Choi and Salem,[45] silicon nitride with equiaxed grains does not exhibit any R-curve behavior and has a low fracture toughness. Becher et al.[44] observed that unreinforced equiaxed silicon nitride exhibited the least R-curve response with a steady-state toughness of only 3.5 MPa $m^{1/2}$. In general, fracture resistance in whisker-reinforced composites is comprised of contributions from both matrix and whisker reinforcement effects, as in the case of Si_3N_4 whisker-reinforced silicon nitride.[46] Therefore, there is potential to further improve the fracture toughness of the silicon nitride–silicon oxynitride in situ composites if the β-Si_3N_4 matrix can offer effective additional toughening mechanisms. Such coupled-toughness behavior is possible in the present composites when we take measures, such as heat treatment in an overpressured nitrogen atmosphere, to increase the grain size and aspect ratio of β-Si_3N_4 grains. An improvement in fracture toughness from 2.9 to 4.3 MPa $m^{1/2}$ has been observed in a fine-grained β-silicon nitride which was annealed at 1800 °C for 60 min in a 1 MPa N_2 atmosphere.[47]

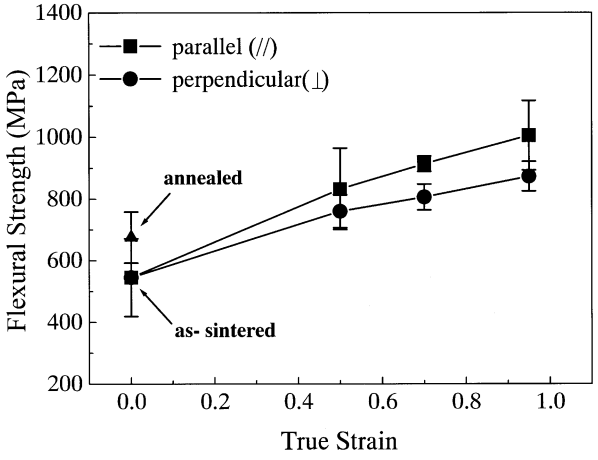

Fig. 7. Measured flexural strength as a function of true compressive strain.

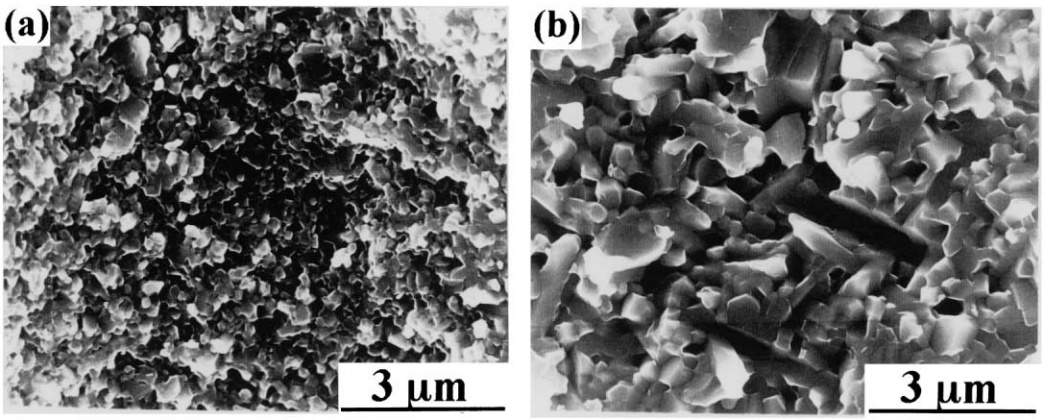

Fig. 8. Fractographs of (a) as-sintered sample and (b) sample deformed to 0.70.

3.4. Flexural strength

Fig. 7 shows flexural strengths of the deformed samples as a function of true strain. The strength of the as-annealed material is also given for comparison. Note that the flexural strength increases monotonously as the compressive strain increases, being 545±126 MPa for the as-sintered material, and 1005±112 MPa (//) and 873±48 MPa (⊥) for the sample deformed to 0.95. The increment in strength for the deformed samples is obviously the result of the significant microstructure evolutions during deformation and subsequent annealing, such as the formation of elongated Si_2N_2O grains, texture development in Si_2N_2O and β-Si_3N_4 and the slight coarsening of the fine-grained β-Si_3N_4 matrix. These can be seen in the fracture surface observations as shown in Fig. 8. Clearly, the as-sintered sample shows a smooth, transgranular topography and apparent equiaxed grain morphology, whereas the composites display a rough, intergranular topography and fibrous morphology.

It is worth mentioning that the as-annealed sample and the sample deformed to 0.55 possess comparable amounts of Si_2N_2O, at about 15 vol.%, but the annealed sample has a lower strength value of 675±83 MPa than the deformed sample which has strengths of 832±132 MPa (II) and 760±54 MPa (⊥). This highlights the contribution of texture development in Si_2N_2O and β-Si_3N_4 to the improvement of flexural strength as the deformed sample is textured. Anisotropy in strength is also present for the deformed samples. The value of the flexural strength measured with the tensile surface parallel to the stress axis is about 10–15% higher than that measured with the tensile surface perpendicular to the stress axis. The presence of the strength anisotropy in the deformed materials is a result of the texture development in Si_2N_2O and β-Si_3N_4. The anisotropy tends to be more pronounced with increasing strain since the degree of texture is greatly dependent on the strain.

The flexural strength of the silicon nitride–silicon oxynitride in situ composites is comparable to that of self-reinforced silicon nitrides. This means that incorporation of silicon oxynitride into the β-silicon nitride matrix does not reduce the strength, but actually enhances it because the elongated silicon oxynitride grains facilitate the crack deflection process, as evidenced in Figs. 5(b) and 8(b). This result is in direct contrast to that reported for O′ + β′-sialon ceramics by Xu et al.[23] They claimed that O′-sialon (a solid solution of Si_2N_2O) introduced into the β-sialon matrix not only reduced the fracture toughness but also decreased the flexural strength (i.e. 376 MPa, about 40% lower than that of the β-sialon matrix). This strength degradation was ascribed to the large size of O′ grains (20–30 μm in length) and the α-Si_3N_4 inclusions, which substantially reduced the strength of the O′ crystals. In addition, the O′ + β′-sialon composite contained 63% O′-sialon and showed a cleavage-like fracture nature of O′ grains, which differs greatly from our materials. Moreover, the elongated O′-sialon grains were randomly orientated in the O′ + β′-sialon composite, while the Si_2N_2O grains are highly textured in the present materials.

4. Conclusions

1. Silicon nitride–silicon oxynitride in situ composites were produced by superplastic deformation at 1600 °C under 40 MPa and subsequent annealing at 1750 °C for 30 min. The composites exhibited a microstructure of elongated Si_2N_2O grains dispersed in a fine-grained β-Si_3N_4 matrix.

2. The mechanical properties of the in situ composites were strain dependent and enhanced as a consequence of microstructure evolutions such as the in situ development of Si_2N_2O, texture formation and the coarsening of β-Si_3N_4 during superplastic deformation and subsequent annealing.

3. Property anisotropies were observed due to the textured microstructure.

Acknowledgements

We are grateful to Dr. T. Nishimura for assistance with the experiments and to Mr. H. Emoto for providing the ultrafine β-Si_3N_4 powder. Financial support for R.J. Xie was provided by the Science and Technology Agency (STA) of Japan.

References

1. Chen, I.-W. and Xue, L. A., Development of superplastic structural ceramics. *J. Am. Ceram. Soc.*, 1990, **73**, 2585–2609.
2. Wakai, F., Kodama, Y., Sakaguchi, S., Murayama, N., Izaki, K. and Niihara, K., A superplastic covalent crystal composite. *Nature (London)*, 1990, **344**, 421–423.
3. Wu, X. and Chen, I. W., Exaggerated texture and grain growth in a superplastic SiAlON. *J. Am. Ceram. Soc.*, 1992, **75**, 2733–2741.
4. Chen, I.-W. and Huang, S. L., Shear thickness creep in superplastic SiAlON ceramics. *J. Am. Ceram. Soc.*, 1992, **75**, 1073–1079.
5. Hwang, S. L. and Chen, I. W., Superplastic forming of SiAlON ceramics. *J. Am. Ceram. Soc.*, 1994, **77**, 2575–2585.
6. Rosenflanz, A. and Chen, I. W., Classical superplasticity of SiAlON ceramics. *J. Am. Ceram. Soc.*, 1997, **80**, 1341–1352.
7. Rouxel, T., Rossignol, F., Besson, J. L. and Goursat, P., Superplastic forming of an α-phase rich silicon nitride. *J. Mater. Res.*, 1997, **12**, 480–492.
8. Mitomo, M., Hirotsuru, H., Suematsu, H. and Nishimura, T., Fine-grained silicon nitride ceramics prepared from β-powder. *J. Am. Ceram. Soc.*, 1995, **78**, 211–214.
9. Wang, C. M., Mitomo, M., Nishimura, T. and Bando, Y., Grain boundary film thickness in superplastically deformed silicon nitride. *J. Am. Ceram. Soc.*, 1997, **80**, 1213–1221.
10. Zhan, G. D., Mitomo, M., Nishimura, T., Xie, R. J., Sakuma, T. and Ikuhara, Y., Superplastic behavior of fine-grained β-silicon nitride material under compression. *J. Am. Ceram. Soc.*, 2000, **83**, 841–847.
11. Zhan, G. D., Mitomo, M. and Xie, R. J., Deformation mechanisms of superplastic flow in fine-grained beta-silicon nitride ceramics. *Acta. Mater*, 2000, **48**, 2373–2382.
12. Xie, R.M., Mitomo, M. and Zhan, G. D., Superplasticity in a fine-grained beta-silicon nitride containing a transient liquid phase. *Acta. Mater.*, 2000, **48**, 2049–2058.
13. Xie, R. J., Mitomo, M., Zhan, G. D. and Emoto, H., Superplastic deformation in silicon nitride–silicon oxynitride in situ composites. *J. Am. Ceram. Soc.*, 2000, **83**, 2529–2535.
14. Rouxel, T. and Wakai, F., Tensile ductility of superplastic Al_2O_3–Y_2O_3–Si_3N_4/SiC composites. *J. Am. Ceram. Soc.*, 1992, **75**, 2363–2372.
15. Xue, L. A. and Chen, I.-W., Fabrication of mullite body using superplastic transient phase. *J. Am. Ceram. Soc.*, 1992, **75**, 1085–1091.
16. Kondo, N., Ohji, T. and Wakai, F., Strengthening and toughening of silicon nitride by superplastic deformation. *J. Am. Ceram. Soc.*, 1998, **81**, 713–716.
17. Thompson, D. P., Sun, W. Y. and Walls, P. A., O′–β′ and α′–β′ SiAlON ceramics. In *Ceramic Materials and Components for Engines,* ed. W. Bunk and H. Hausner. German Ceramic Society, 1986, pp. 643–649.
18. Greil, P., High temperature strengthening of silicon nitride ceramics. *Sci. Ceram.*, 1987, **14**, 645–651.
19. O'Meara, C., Sjoberg, J. and Dunlop, G., Oxidation of pressureless sintered Si_2N_2O materials. *J. Eur. Ceram. Soc.*, 1991, **7**, 369–378.
20. Ohashi, M., Kanzaki, S. and Tabata, H., Processing, mechanical properties, and oxidation behavior of silicon oxynitride ceramics. *J. Am. Ceram. Soc.*, 1991, **74**, 109–114.
21. Braue, W., Pleger, R. and Luxem, W., Nucleation and growth of Si_2N_2O in Si_3N_4 materials employing different sintering additives. *Key. Eng. Mater.*, 1994, **89–91**, 483–488.
22. Sjoberg, J. and O'Meara, C., The effect of yttria additions on the composition of O′-sialon prepared by pressureless sintering. *J. Eur. Ceram. Soc.*, 1992, **10**, 41–50.
23. Xu, Y., Huang, C. M., Kriven, W. M. and Zangvil, A., Residual α-Si_3N_4 in O′-crystals in CeO_2-doped O′ + β′ SiAlON ceramics. *J. Am. Ceram. Soc.*, 1994, **77**, 2213–2216.
24. Wang, C. M., Emoto, H. and Mitomo, M., Nucleation and growth of silicon oxynitride grains in a fine-grained silicon nitride matrix. *J. Am. Ceram. Soc.*, 1998, **81**, 1125–1132.
25. Tani, E., Umebayashi, S., Kishi, K. and Kobayashi, K., Gas-pressure sintering of Si_3N_4 with concurrent addition of Al_2O_3 and 5wt% rare earth oxide: high fracture toughness Si_3N_4 with fiber-like structure. *Am. Ceram. Soc. Bull.*, 1986, **65**, 1311–1315.
26. Li, C. W. and Yamanis, J., Super-tough silicon nitride with R-curve behavior. *Ceram. Eng. Sci. Proc.*, 1989, **10**, 632–645.
27. Mitomo, M., Toughening of silicon nitride ceramics by microstructure control. In *Proceedings of the 1st International Symposium on the Science of Engineering Ceramics*, ed. S. Kimura and K. Niihara. Ceramic Society of Japan, Tokyo, Japan, 1991, pp. 101–107.
28. Xie, R. J., Mitomo, M., Kim, W. and Kim, Y. W., Texture development in silicon nitride–silicon oxynitride in situ composites via superplastic deformation. *J. Am. Ceram. Soc.*, 2000, **83**, 3147–3152.
29. Goto, Y. and Tsuge, A., Mechanical properties of unidirectionally oriented SiC-whisker-reinforced Si_3N_4 fabricated by extrusion and hot-pressing. *J. Am. Ceram. Soc.*, 1993, **76**, 1420–1424.
30. Hirao, K., Ohashi, M., Brito, M. E. and Kanzaki, S., Processing strategy for producing highly anisotropic silicon nitride. *J. Am. Ceram. Soc.*, 1995, **78**, 1687–1690.
31. Muscat, D., Pugh, M. D., Drew, R. A. L., Pickup, H. and Steele, D., Microstructure of an extruded β-silicon nitride whisker-reinforced silicon nitride composites. *J. Am. Ceram. Soc.*, 1992, **75**, 2713–2718.
32. Mitomo, M., Saito, S., Matsuda, T. and Yonezawa, T., Sintering anisotropy in slip-cast SiC-whisker/Si_3N_4 powder compacts. *J. Mater. Sci.*, 1993, **28**, 5548–5553.
33. Huang, Z. K., Greil, P. and Petzow, G., Formation of silicon oxynitride from Si_3N_4 and SiO_2 in the presence of Al_2O_3. *Ceram. Int.*, 1984, **10**, 14–17.
34. Lewis, M. H., Reed, C. J. and Butler, N. D., Pressureless-sintered ceramics based on the compounds Si_2N_2O. *Mater. Sci. Eng.*, 1985, **71**, 87–94.
35. Mitomo, M., Ono, S., Asami, T. and Kang, S. J. L., Effect of atmosphere on the reaction sintering of Si_2N_2O. *Ceram. Int.*, 1989, **15**, 345–350.
36. Yabuta, K., Nishio, H. and Uematsu, K., Effect of process-related oxidation on transition liquid-phase sintering of β′–O′ sialon ceramics. *J. Jpn. Ceram. Soc.*, 1995, **103**, 1046–1050.
37. Yabuta, K. and Nishio, H., Effect of heating rate on transition liquid-phase sintering of β′–O′ sialon ceramics. *J. Jpn. Ceram. Soc.*, 1995, **103**, 1302–1304.
38. Emoto, H., Mitomo, M., Wang, C. M., Hirosturu, H. and Inaba, T., Fabrication of silicon nitride–silicon oxynitride in-situ composites. *J. Eur. Ceram., Soc.*, 1998, **18**, 527–533.
39. Marshall, D. B., Controlled flaws in ceramics: a comparison of knoop and vickers indentation. *J. Am. Ceram. Soc.*, 1983, **66**, 127–131.
40. Clarke, D. R., On the equilibrium thickness of intergranular glass phases in ceramic materials. *J. Am. Ceram. Soc.*, 1987, **70**, 15–22.

41. Kleebe, H. J., Cinibulk, M. K., Cannon, R. M. and Ruhle, M., Statistical analysis of the intergranular film thickness in silicon nitride ceramics. *J. Am. Ceram. Soc.*, 1993, **76**, 1969–1977.
42. Faber, K. T. and Evans, A. G., Crack deflection process: I. Theory. *Acta Mater.*, 1983, **31**, 565–576.
43. Becher, P. F., Microstructural design of toughened ceramics. *J. Am. Ceram. Soc.*, 1991, **74**, 255–269.
44. Becher, P. F., Sun, E. Y., Plucknett, K. P., Alexander, K. B., Hsueh, C. H., Lin, H. T., Waters, S. B., Westmoreland, C. G., Kang, E. S., Hirao, K. and Brito, M., Microstructural design of silicon nitride with improved fracture toughness: I, effects of grain shape and size. *J. Am. Ceram. Soc.*, 1998, **81**, 2821–2830.
45. Choi, S. R. and Salem, J. A., Strength, toughness and R-curve behavior of SiC whisker-reinforced composite Si_3N_4 with reference to monolithic Si_3N_4. *J. Mater Sci.*, 1992, **27**, 1491–1498.
46. Chu, C. Y. and Singh, J. P., Mechanical properties and microstructure of Si_3N_4-whiskers-reinforced Si_3N_4-matrix composites. *Ceram. Eng. Sci. Proc.*, 1990, **11**, 709–720.
47. Sato, H., Mitomo, M., Nishimura, T. and Emoto, H., Mechanical properties of fine-grained silicon nitride ceramics. *J. Jpn. Ceram. Soc.*, 1998, **106**, 203–207.